JOURNAL OF AIRCRAFT
Vol. 46, No. 1, January–February 2009

Characterizing Stability and Control of Subscale Aircraft from Wind-Tunnel Dynamic Motion

S. D. Carnduff,* S. D. Erbsloeh,† A. K. Cooke,‡ and M. V. Cook§
Cranfield University, Bedfordshire, England MK43 0AL, United Kingdom

DOI: 10.2514/1.36730

This paper outlines a process of determining the stability and control characteristics of small-scale aircraft from wind-tunnel experiments which aim to emulate flight tests. Scaled aircraft models with representative control surfaces are flown in semifree flight on a test rig allowing motion in 4 degrees of freedom. The motion is measured and system identification and parameter estimation techniques are used to obtain a mathematical description of the dynamics of the model. Previous work has relied on the use of potentiometers to measure the model's attitude about its pivot point with other motion variables being generated analytically using these measurements and well-known kinematic relationships. However, it is now possible to mount sensors within the model as advances in technology have produced microelectromechanical system packages of small size, lightweight, low cost, and low power consumption. The current work is investigating the effectiveness of using microelectromechanical system inertial sensors to measure motion of the model. An example of the system identification process carried out on a one-twelfth scale BAe Hawk model is also presented. Parameter estimation is performed in the frequency domain using the equation error and output error methods.

Nomenclature

$\mathbf{A}$	=	state matrix
$\mathbf{B}$	=	input matrix
$\mathbf{C}$	=	output matrix
$\mathbf{D}$	=	direct matrix
g	=	acceleration due to gravity
J	=	cost function
j	=	imaginary number
p	=	roll rate
q	=	pitch rate
r	=	yaw rate
s	=	standard error, Laplace operator
v	=	sideslip velocity
w	=	normal velocity
α	=	angle of attack
β	=	angle of sideslip
ζ	=	rudder input
η	=	elevator input
Θ	=	parameter vector
θ	=	pitch attitude
ξ	=	aileron input
ϕ	=	roll attitude
ψ	=	yaw attitude

Superscripts

T	=	transpose
$\hat{}$	=	estimate
$\tilde{}$	=	Fourier transform
$\dot{}$	=	time derivative
†	=	complex conjugate transpose

Presented as Paper 196 at the 46th AIAA Aerospace Sciences Meeting and Exhibit, Reno, Nevada, 7–10 January 2008; received 18 January 2008; revision received 13 August 2008; accepted for publication 15 September 2008. Copyright © 2008 by Cranfield University. Published by the American Institute of Aeronautics and Astronautics, Inc., with permission. Copies of this paper may be made for personal or internal use, on condition that the copier pay the $10.00 per-copy fee to the Copyright Clearance Center, Inc., 222 Rosewood Drive, Danvers, MA 01923; include the code 0021-8669/09 $10.00 in correspondence with the CCC.

*Research Student, Department of Aerospace Sciences. Student Member AIAA.
†Research Officer, Department of Aerospace Sciences. Member AIAA.
‡Senior Lecturer, Department of Aerospace Sciences.
§Head of Dynamics, Simulation and Control Group, Department of Aerospace Sciences.

I. Introduction

ACCURATE mathematical models of aircraft dynamics are required for a number of applications, including flight control system design, simulator development, and flying qualities analysis. Although flight dynamics information, in the form of stability and control derivatives, can be established in a number of ways, experimental techniques, such as wind-tunnel testing, will provide mathematical models with the highest degree of fidelity.

An established method for determining aerodynamic derivatives from wind-tunnel experiments is to mount a scaled model of the aircraft onto a test rig and observe the model's free or forced oscillatory response [1]. By connecting the rig to a suitable balance, the derivatives of forces and moments with respect to the motion variables can be obtained. A different approach to the problem is to emulate flight testlike experiments in the wind-tunnel environment [2–9]. A dynamically scaled model with representative control surfaces is mounted on the test rig and flown in semifree flight. Specific inputs are applied to the control surfaces, which are deflected using miniature servoactuators, and the resultant response of the model is measured using motion sensors. The stability and control derivatives can then be extracted from the input/output data using system identification and parameter estimation techniques similar to those used in the flight test environment.

In the past, a drawback of the technique has been the lack of accurate inertial sensors, such as accelerometers and rate gyros, which were small enough to fit within the aircraft model. To overcome this problem, potentiometers were used to measure the model's attitude about its pivot point, and data for other motion variables were generated analytically using the attitude measurements and kinematic relationships. However, this lack of redundancy in the sensors means that any errors in the output of the potentiometers will directly affect the values of other motion variables and, ultimately, the estimates of the stability and control derivatives. The use of accelerometers and gyros for wind-tunnel experiments was reported by Rajamurthy [9]. However, because of their weight, they were only used to check the accuracy of the potentiometers and were removed before any experiments had been conducted.

A major advancement in sensor technology over the last two decades has been the rapid development of inertial sensors based on

microelectromechanical systems (MEMS) technology. This development has been driven by the widespread use of these devices by the automotive industry [10]. The main advantages of these sensors are their small size, lightweight, low cost, and low power consumption. The main drawback of MEMS sensors at present is their poor accuracy in comparison with more mature sensor technologies. In addition, they exhibit noisier outputs and have more significant bias and drift characteristics. With the current application in mind, however, MEMS are the only class of inertial sensors that are small enough to be housed in a scaled wind-tunnel model. The gap in accuracy between MEMS sensors and other sensor types has also narrowed over recent years and it is predicted that the quality of MEMS sensors will continue to improve in the future.

Current work is focusing on the development of a wind-tunnel facility using MEMS sensor technology. The primary interest of the research is the capability to obtain stability and control derivative information of full-sized aircraft, particularly unmanned aerial vehicle (UAV) configurations, rapidly and at a low cost. Determination of the flight dynamics properties through experimental means is especially important for UAVs. These aircraft tend to have unusual airframe configurations, making empirical methods of estimating the stability and control derivatives, such as DATCOM [11] and ESDU [12], less reliable. Another benefit of the facility is that much of the instrumentation used in the wind-tunnel models, such as the sensors and servoactuators, is similar to that typically employed in small UAVs. A parallel research project being conducted at Cranfield is concerned with flight testing small-scale UAVs; hence the wind-tunnel facility provides a means of gaining experience with these technologies before they are used in free-flying applications. This research is being carried out as part of the Flapless Air Vehicle Integrated Industry Research (FLAVIIR) program, which is jointly funded by BAE Systems and the United Kingdom's Engineering and Physical Science Research Council (EPSRC). The broad aim of the project, which is a collaboration between 10 university partners, is to develop technologies for UAVs with unconventional control surfaces and the program will culminate with the flight of demonstrator UAV, shown in Fig. 1. As part of the aircraft's development, a scale model of the UAV has been tested in the dynamic wind-tunnel facility at Cranfield using the method described in this paper.

The next section of this paper gives an overview of the dynamic wind-tunnel facility, followed by a description of the instrumentation and data acquisition process in Sec. III. Relevant dynamic scaling laws are then summarized in Sec. IV and the equations of motion for models tested in the facility are discussed in Sec. V. Section VI describes the system identification and parameter estimation process carried out on a one-twelfth scale BAe Hawk model and the results of the analysis are presented in Sec. VII.

II. Dynamic Wind-Tunnel Facility Description

The dynamic wind-tunnel facility at Cranfield University was originally developed in the early 1980s [5,13] and has been used to investigate a number of aircraft configurations [6,8]. Figure 2 shows the test rig with a one-twelfth scale model of the BAe Hawk, which has been used as a platform for testing the facility's upgraded instrumentation and hardware. The design of the rig is relatively simple, with the aircraft model suspended on a stiff vertical rod, which is itself attached to a Dexion framework. The vertical rod passes through a gimbal mechanism within the model, shown in Fig. 3a, that allows the aircraft to rotate in roll, pitch, and yaw and to translate vertically along the axis of the rod. The rig therefore allows investigation of 4 degrees of freedom (DOF) of motion. The range of motion permitted is ± 30 deg rotation in roll and pitch, 360 deg in yaw, and a translation of approximately 0.75 m in the vertical axis. The gimbal and rod assembly was made as small and as light as possible to minimize their influence on the aircraft model, and the gimbal incorporates precision ballraces and linear ball bearings to minimize frictional effects. The test rig is designed to be placed in an open section wind tunnel. The tunnel used for the experiments described below has a working section of 1.5×1.1 m and a maximum speed of 40 m/s. The maximum wing span of the model is limited to around 0.9 m.

Fig. 1 FLAVIIR demonstrator UAV.

Fig. 2 Dynamic wind-tunnel rig with a one-twelfth scale BAe Hawk model.

III. Instrumentation

An off-the-shelf inertial measurement unit (IMU), shown in Fig. 3b, is used to record the model motion. The IMU comprises a set of three MEMS accelerometers, three MEMS rate gyros, and three solid state magnetometers. The ranges of these sensors are ± 2 g, ± 150 deg/s, and ± 2 G, respectively. A Kalman filter is used to fuse data from the sensors and provide a measure of the model's attitude angles. The procedure and the equations used to accomplish this can be found, for example, in [14]. Analog-to-digital conversion of the measured signals is 16-bit binary, and data can be sampled from each of the sensors at a maximum rate of 100 Hz. The unit is very compact, with dimensions of $5.7 \times 4.5 \times 1.1$ cm and lightweight at only 33 g.

Control surface deflections are achieved using miniature servoactuators (also shown in Fig. 3b), based on radiocontrolled aircraft technology. These are physically connected to the relevant control surfaces using standard model control linkages. Commands to the servoactuators are transmitted from a computer "ground station" through a low power 2.4-GHz wireless link. The resultant motion recorded by the sensors is then sent back via the wireless network to the ground station. This avoids the need to connect wires

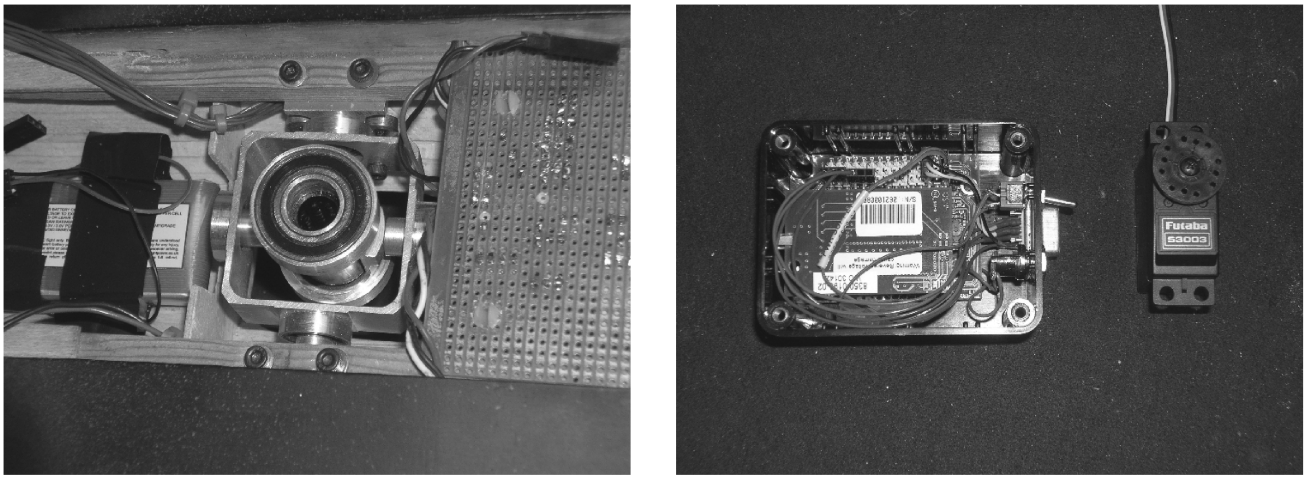

a) Gimbal mechanism **b) MEMS IMU and miniature servoactuator**

Fig. 3 Dynamic wind-tunnel hardware.

and cabling to the model or test rig, removing a possible source of aerodynamic interference.

IV. Dynamic Scaling Laws

If a valid comparison between wind-tunnel tests and the full-sized aircraft is to be made, a model tested in the wind tunnel must be properly scaled. That is, the model and the full-sized aircraft must be geometrically, kinematically, and dynamically similar. To achieve this, the following nondimensional parameters must be considered in the design of appropriate wind-tunnel tests:

1) Mach number: $M = V/a$, where V denotes velocity and a is the local speed of sound.

2) Strouhal number: $Sr = \omega l/V$, where ω is the oscillation frequency and l is the characteristic length of the aircraft/model.

3) Froude number: $Fr = V/\sqrt{gl}$.

4) Reynolds number: $Re = \rho V l/\mu$, where ρ is the atmospheric density and μ is dynamic viscosity.

5) Relative density: $RD = 2m/(\rho S l)$, where S is the wing area.

6) Relative radius of inertia/gyration: $K = (r_g/l)^2$, where r_g is the radius of gyration.

Other important scaling laws are as follows: 1) model geometric scale factor: $\lambda = l_m/l_a$, 2) velocity: V_m/V_a, 3) atmospheric density: ρ_m/ρ_a, 4) mass: $m_m/m_a = \lambda^3 \rho_m/\rho_a$, 5) inertia: $I_m/I_a = \lambda^5 \rho_m/\rho_a$, 6) gravity: $g_m/g_a = V_m/(\lambda V_a)$, 7) time: $\tau = t_m/t_a = \lambda V_a/V_m$, where the subscripts m and a indicate model and full-sized aircraft parameters, respectively.

Simultaneous matching of the nondimensional parameters and scaling laws is difficult to achieve in practice. For example, it is impossible to simulate the Reynolds number correctly without using models of a similar size to the full-sized aircraft or using a medium in the wind tunnel with different viscous properties to air [5]. This problem is partly accounted for by using trip wires on the model to promote turbulent flow.

An advantage when wind-tunnel testing UAV configurations is that unmanned aircraft, by their nature, tend to be much smaller than manned aircraft. Therefore, models of UAVs will be much closer in size to the full-sized vehicle and the adverse effects of failing to match the scaling laws will be reduced.

V. 4 DOF Equations of Motion

For the research carried out thus far, it has been assumed that motion of the model on the rig can be approximated by small perturbations from an initial trim condition and that longitudinal and lateral/directional motion can be decoupled. Equations describing the model's dynamics are referenced to a Cartesian axis system with the origin fixed at a given point within the model. The most convenient choice for the axes origin is the location of the gimbal, as this is the point about which the model maneuvers. The wind-tunnel velocity vector is assumed to act parallel to the ground, so the model's pitch attitude θ and angle of attack α are the same. Also, when the model is at wings level, a positive yaw angle ψ (nose to starboard) equates to a negative sideslip angle β.

In comparison to the longitudinal motion of an equivalent free-flying aircraft, axial velocity perturbations experienced by the model will be suppressed by the rig. It is, therefore, not possible to simulate the phugoid, as axial velocity is a dominant variable in this particular mode of motion. However, it is possible to use the rig to simulate the short period, a mode of motion characterized by oscillations in heave and pitch, which are variables unconstrained by the rig. The inability to simulate the phugoid is not considered a disadvantage as it is usually the short period dynamics that are of particular interest when, for example, designing stability augmentation and flight control systems and performing handling qualities analysis [15].

The longitudinal equations of motion of the model are therefore expressed in state space form as

$$\begin{bmatrix} \dot{w} \\ \dot{q} \end{bmatrix} = \begin{bmatrix} z_w & z_q \\ m_w & m_q \end{bmatrix} \begin{bmatrix} w \\ q \end{bmatrix} + \begin{bmatrix} z_\eta \\ m_\eta \end{bmatrix} \eta \tag{1}$$

where w is the model's normal velocity, q is its pitch rate, and η denotes elevator deflection. As noted above, these variables represent perturbations from initial trim values. The stability and control derivatives z_w, z_q, z_η, m_w, m_q, and m_η are given in concise form (see Cook [15]). As expected from the description of the constrained longitudinal motion above, Eq. (1) is identical to the short period approximation of a free-flying aircraft.

In practice, wind-tunnel models tend to be very responsive in heave and will quickly hit any end stops on the vertical rod. This precludes safe testing in all 4 degrees of freedom without some form of closed-loop height control system. Although such a system had been successfully implemented in previous work [16], it has yet to be reproduced with the updated sensors and instrumentation due to difficulties in obtaining an accurate value of height wirelessly. Consequently, the experiments carried out thus far and outlined in Sec. VI have been performed with the model constrained in the z axis, thus reducing the longitudinal equations of motion to

$$\begin{bmatrix} \dot{w} \\ \dot{q} \end{bmatrix} = \begin{bmatrix} 0 & V_T \\ m_w & m_q \end{bmatrix} \begin{bmatrix} w \\ q \end{bmatrix} + \begin{bmatrix} 0 \\ m_\eta \end{bmatrix} \eta \tag{2}$$

where V_T is the wind-tunnel velocity.

In the lateral/directional plane, the principal difference between motion of the model and the aircraft is that the rig suppresses lateral translation. This means that only the roll mode and dutch roll motion can be observed. As with the longitudinal case, this is not viewed as a major drawback as it is generally the short term roll subsidence and

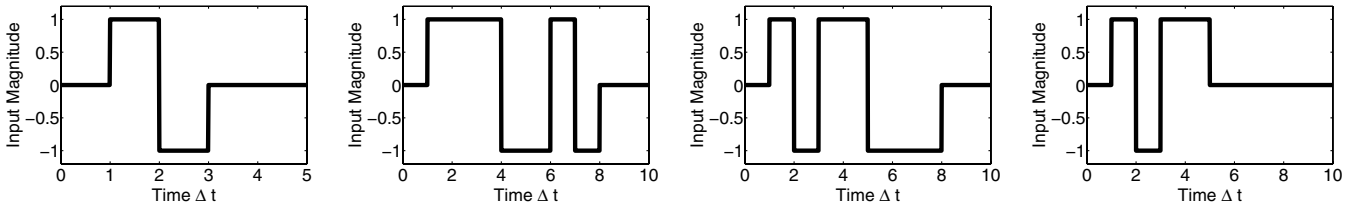

a) Doublet **b) 3-2-1-1** **c) 1-1-2-3** **d) 1-1-2**

Fig. 4 Multistep inputs tested during experiments.

dutch roll modes, rather than the long term spiral mode, that are of interest.

The roll mode of the wind-tunnel model can be approximated by the single degree of freedom equation

$$\dot{p} = l_p p + l_\xi \xi \tag{3}$$

where p is the model's roll rate, ξ represents the input to the ailerons, and l_p and l_ξ are the stability and control derivatives. The dutch roll dynamics may be described by the expression,

$$\begin{bmatrix} \dot{v} \\ \dot{r} \end{bmatrix} = \begin{bmatrix} 0 & -V_T \\ n_v & n_r \end{bmatrix} \begin{bmatrix} v \\ r \end{bmatrix} + \begin{bmatrix} 0 \\ n_\zeta \end{bmatrix} \zeta \tag{4}$$

where v denotes sideslip velocity, r is yaw rate, and ζ represents the rudder input. Because of the suppression of any lateral motion, the sideforce derivatives with respect to v and ζ are zero.

The experiments carried out thus far have used a conventional airframe configuration and have been performed at low angles of attack. In this case, the dynamics are linear and can be described by the equations outlined above. However, a goal is to use the facility in the future to investigate more unusual aircraft configurations and to fly models at higher angles of attack and sideslip. These conditions can be hazardous and difficult to sustain in the flight test environment. Therefore, the aim is to use the facility to safely investigate more complex, nonlinear flight conditions.

VI. Experimental Procedure

This section outlines the system identification and parameter estimation process applied to the one-twelfth scale model of the BAe Hawk, shown in Fig. 2. The goal of the experiments was simply to gather data on which system identification and parameter estimation algorithms could be tested, rather than to obtain information relevant to the full-sized aircraft. Hence, the model mass and inertias were not scaled appropriately before the tests. Some practical considerations for the experiments are described below and the results of the analysis are presented in Sec. VII. The results presented in this paper were obtained from tests conducted at a wind-tunnel speed of 30 m/s and an angle of attack of 0 deg. The data were analyzed using a software tool set designed to provide rapid and efficient estimation in situ. Some parameter estimation algorithms contained in the MATLAB software package *SIDPAC* (System Identification Programs for Aircraft) developed at NASA Langley Research Center by Klein and Morelli [17] and Morelli [18], as well as algorithms written at DLR, German Aerospace Research Center, by Jategaonkar [19] form the basis of this tool set.

A. Input Design

The first step in the experimental process was the design of suitable inputs to the control surfaces to excite the dynamics of interest and, for this, a simple multistep approach was chosen. A number of multistep input shapes can be used [17,19] but four types of inputs, shown in Fig. 4, were tested in the experiments: doublet, 3-2-1-1, 1-1-2-3, and 1-1-2.

The pulse width of the inputs was selected using the following rule of thumb [17]:

$$\Delta t = \frac{0.35}{f_n} \tag{5}$$

where f_n is the predicted natural frequency of the aircraft in Hertz. For the Hawk model, the values of f_n were obtained using an empirical analysis by Malik [5]. Based on this a priori knowledge, the required values of Δt for the elevator and rudder inputs were set at 0.3 s. For practical reasons, Δt was reduced to 0.15 s for the ailerons as the model was very responsive in roll [5,8]. The value of Δt selected ensured that the model did not reach the ± 30 deg roll limits permitted by the rig. Computer generated inputs were used as these values of Δt were very small making it difficult to apply the inputs manually with any degree of accuracy. A similar problem often occurs when flight testing small UAVs. Computer generated inputs are also preferred as the visual and motion cues usually present in piloted flight are not available when operating the vehicle remotely making manual input difficult to apply consistently [20].

An observation from the experiments was that, when applying a 3-2-1-1 input to the elevator, initially the "3" step caused the model to

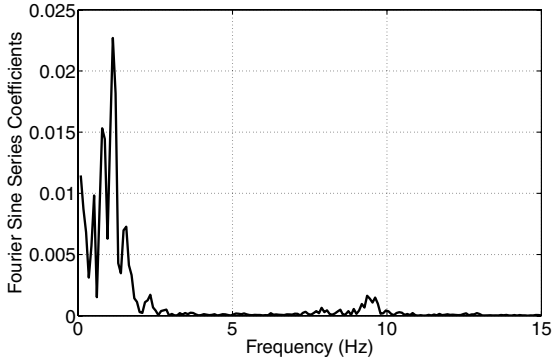

Fig. 6 Fourier sine series coefficients of the angle of attack signal against frequency.

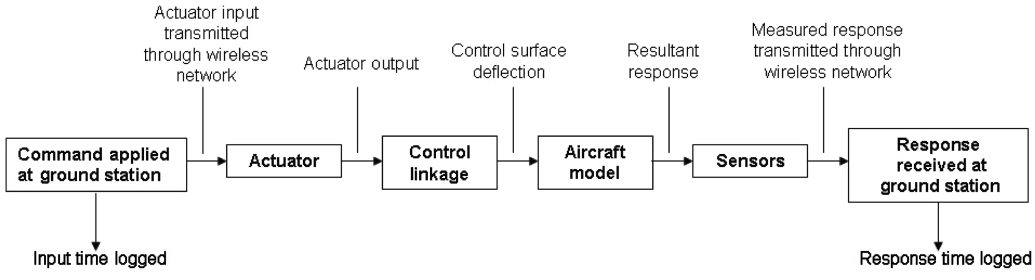

Fig. 5 Transmission and logging of data.

Table 1 Estimates of gyro error parameters

	$\hat{\Theta}$	$s(\hat{\Theta})$	$100[s/\lvert\hat{\Theta}\rvert]$
λ_p	0.1254	1.34×10^{-3}	1.07
b_p	0.0048	3.37×10^{-4}	7.02
λ_q	0.0273	2.49×10^{-3}	9.13
b_q	−0.0030	2.46×10^{-4}	8.19
λ_r	−0.0723	5.41×10^{-3}	7.48
b_r	−0.0088	1.52×10^{-4}	1.73

pitch up to high angles of attack, leading to a cross coupling into rolling motion. This coupling could only be prevented by reducing the pulse amplitude. A similar situation was encountered when applying the 1-1-2-3 inputs. It was found that if the input was restricted to a 1-1-2, larger amplitude inputs could be applied without the model undergoing any undesirable lateral–directional motion.

B. Data Compatibility Check

Before using the data for parameter estimation, a compatibility check was performed on the measurements. Only a comparison between the angular rates and the attitudes was possible as all measurements were provided by the IMU, and so no check was made on the accelerometer data. However, this is not viewed as critical because, for the 3 DOF case, the model is only permitted to undergo rotary motion and only the angular rate and attitude measurements are used for the subsequent parameter estimation step. The kinematic relationships relating the two sources of data are

$$\dot{\phi} = p + (q \sin\phi + r \cos\phi) \tan\theta \tag{6}$$

$$\dot{\theta} = q \cos\phi - r \sin\phi \tag{7}$$

$$\dot{\psi} = (q \sin\phi + r \cos\phi) \sec\theta \tag{8}$$

where ϕ, θ, and ψ are the roll, pitch, and yaw angles, respectively, whereas p, q, and r are the roll, pitch, and yaw rates. However, as it is assumed that the motion under analysis can be represented as small perturbations about trim, Eqs. (6–8) reduce to the linear form,

$$\dot{\phi} = p \tag{9}$$

$$\dot{\theta} = q \tag{10}$$

$$\dot{\psi} = r \tag{11}$$

For each of the measurements, the following general sensor model can be proposed:

$$y_m = (1 + \lambda_y) y + b_y \tag{12}$$

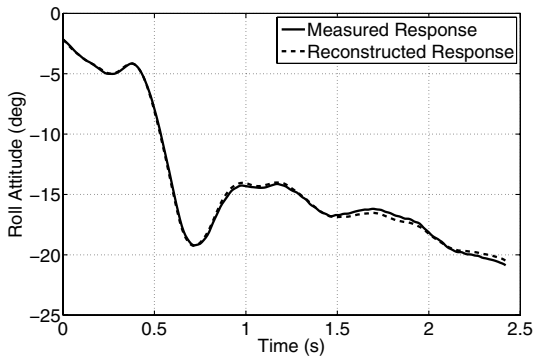

Fig. 7 Measured and reconstructed roll attitudes.

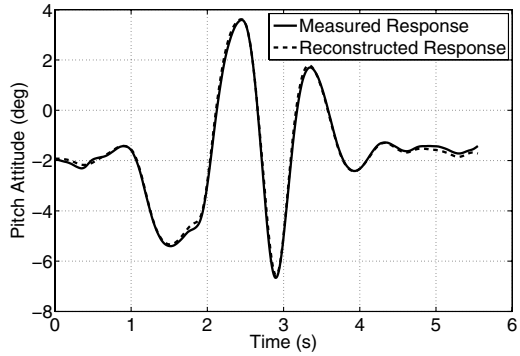

Fig. 8 Measured and reconstructed pitch attitudes.

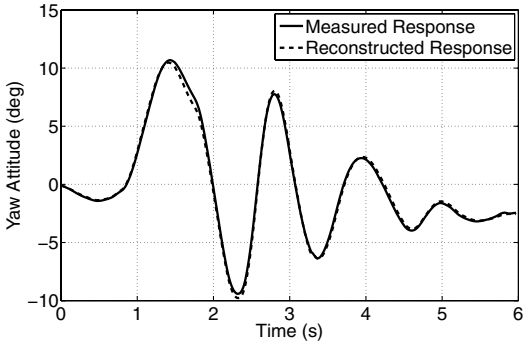

Fig. 9 Measured and reconstructed yaw attitudes.

where y_m denotes the measurement of the true value of variable y, λ_y is the scale factor error, and b_y is the bias error. The aim of the data compatibility check is to then estimate the bias and scale factors errors, which can be removed before parameter estimation.

Along with systematic errors, gyro measurements are also likely to contain random measurement noise. If the noise is negligible, then the system can be treated as deterministic, and the estimates of the instrumentation errors can be obtained using the time domain, maximum likelihood output error method [17,19,21]. On the other hand, significant noise in the gyros will appear as process noise and the problem becomes a stochastic one. In this case, the noise can be removed by filtering or smoothing the input variables before using the output error method. Alternatively, an approach based on an extended Kalman filter can be used.

C. Parameter Estimation

Having accounted for the bias and scale factor errors in the data, estimates of the stability and control derivatives were made. This required knowledge of the control surface deflections, which for full-sized aircraft are usually measured with potentiometers or linear variable differential transducers [19]. However, due to the small size

Table 2 Estimates of parameters

	$\hat{\Theta}$	$s(\hat{\Theta})$	$100[s/\lvert\hat{\Theta}\rvert]$	Empirical estimate
V_T	29.0356	0.2338	1.20	30.00
m_w	−1.7897	0.0829	5.24	−1.64
m_q	−3.7925	0.4355	10.28	−4.01
m_η	−2.1343	0.1595	7.16	−2.60
τ_η	0.3125	0.0067	2.55	——
V_T	30.5353	0.2337	0.80	30.00
n_v	0.8824	0.0289	2.91	1.28
n_r	−1.6654	0.1843	10.26	−1.53
n_ζ	−0.6616	0.0377	4.93	−0.67
τ_ζ	0.2847	0.0061	1.89	——
l_p	−3.7253	0.4921	13.21	−5.32
l_ξ	−4.3589	0.4742	4.85	−3.43
τ_ξ	0.2009	0.0053	2.63	——

Table 3 Correlation coefficients for pitch parameters

	V_T	m_w	m_q	m_η	τ_η
V_T	1	0.40	0.19	0.15	0.01
m_w	——	1	0.31	0.49	0.56
m_q	——	——	1	0.69	0.45
m_η	——	——	——	1	0.41
τ_η	——	——	——	——	1

Table 4 Correlation coefficients for yaw parameters

	V_T	n_v	n_r	n_ζ	τ_ζ
V_T	1	0.03	0.11	0.01	0.00
n_v	——	1	0.02	0.19	0.31
n_r	——	——	1	0.54	0.44
n_ζ	——	——	——	1	0.18
τ_ζ	——	——	——	——	1

Table 5 Correlation coefficients for roll parameters

	l_p	l_ξ	τ_ξ
l_p	1	0.49	0.42
l_ξ	——	1	0.45
τ_ζ	——	——	1

of the wind-tunnel model, it was not practical to measure the control surface positions in this manner. This situation has also been encountered with small-scale UAVs [20]. Instead, the control surface deflections were determined by recording the commands to the actuators and using knowledge of the actuator and the control linkage dynamics. For the Hawk model, the linkages were represented as simple gains and the actuator characteristics were obtained by applying frequency sweeps to the devices in isolation. Using input/output information from a number of repeat runs, the actuators were characterized by the following second-order transfer function:

$$\frac{y(s)}{\delta(s)} = \frac{482.657}{s^2 + 29.432s + 482.657} \tag{13}$$

where δ and y are the actuator command and output, respectively. Position and rate limits of the actuators were also accounted for. The accuracy of the control surface deflections determined using the above approach is dependent on the fidelity of the actuator and control linkage models. There can be significant nonlinearities in the actuator behavior, particularly for the small, low-cost devices, and their performance will vary under different loading conditions. The control linkages can also introduce nonlinear effects due to hysteresis and dead bands. Although the above approach worked well for this research, direct measurement of the control surface positions is preferable if possible.

From Eq. (13), the actuator natural frequency is calculated to be approximately 22 rad/s. This bandwidth is very low, when compared to actuators typically used on full-sized aircraft, and illustrates that the tradeoff made for reduced cost, size, and weight is usually a decrease in performance. It is noted that as the size of an aircraft decreases, its natural frequency will increase; therefore, the respective bandwidths of the airframe and subsystems will be closer in magnitude, leading to a greater need to account for the subsystem dynamics in the analysis.

As well as estimating the model's stability and control derivatives, it was necessary to estimate an equivalent time delay caused principally by the need to transmit and receive data through the digital wireless network. Accurate knowledge of this time delay was important as it has been shown that time shifts in the data lead to degraded estimates of the stability and control derivatives, particularly if the time shift is in the control input [22]. The block diagram in Fig. 5 illustrates the process of transmitting and logging the data. The control inputs were time logged when the user command was applied at the ground station and the resultant response was time logged when the data were received from the sensors. Again, the problem of estimating this time shift would be mitigated if it were possible to measure control surface deflections directly.

The choice was made to perform the parameter estimation step in the frequency domain, which is better suited to the estimation of time delays when compared with time domain approaches [23,24]. A second reason for using the frequency domain was the presence of an undesired structural vibration in the rig, see Fig. 6, which shows a plot of the Fourier sine series coefficients of the angle of attack data against frequency. The coefficients with large amplitudes located at frequencies below 3 Hz belong to the rigid-body dynamics of the model. Above 3 Hz, the amplitudes reduce to a relatively small and constant value, which corresponds to noise in the data. However, as a result of rig vibration the amplitudes increase again at approximately

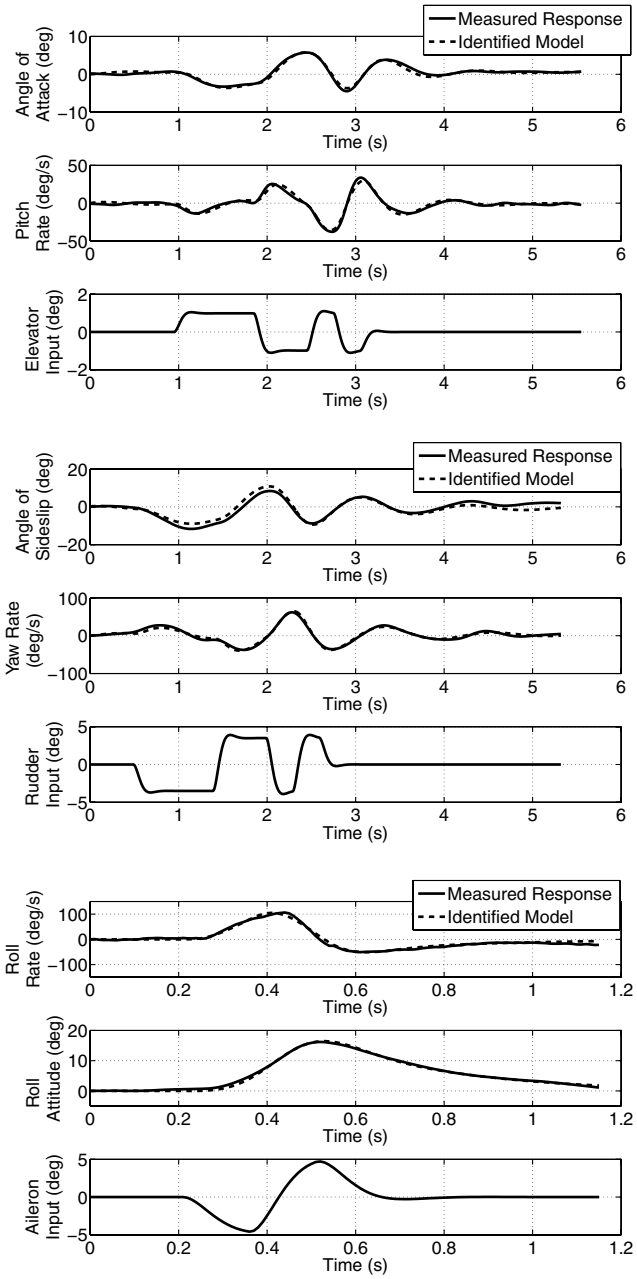

Fig. 10 Time histories of measured and identified responses for 3-2-1-1 inputs to the elevator and rudder and a doublet input to the ailerons.

8 Hz. By performing parameter estimation in the frequency domain, the analysis can be restricted to a given band of frequencies and, thus, the rigid-body dynamics can be isolated from the higher frequency structural vibration.

The data were transformed into the frequency domain using a chirp-z Fourier transform. The lower frequency limit (in Hertz) was chosen as $2/T$, where T is the length of time of the maneuver under analysis. This means that, for each frequency, there will be at least

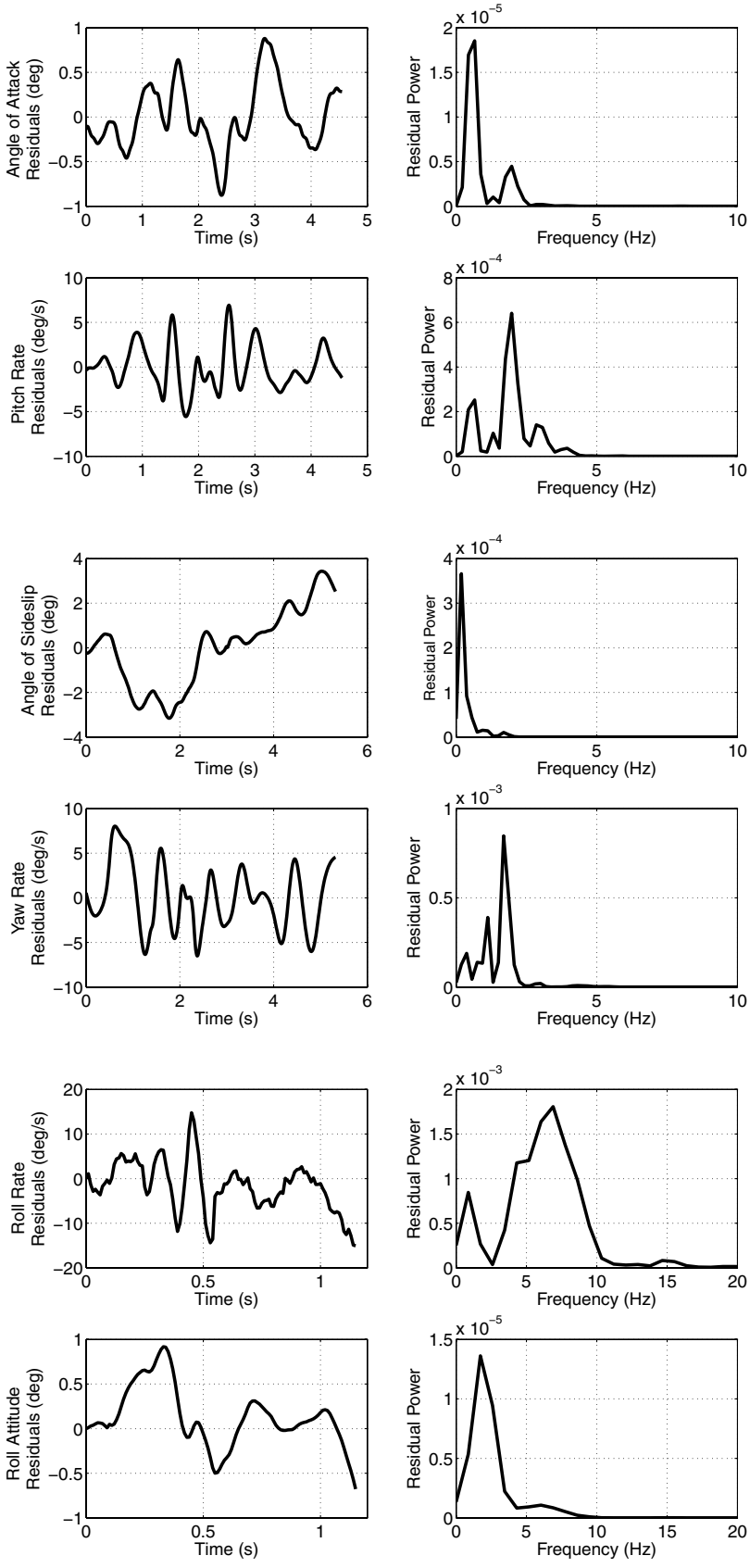

Fig. 11 Modeling residuals and associated power spectrums.

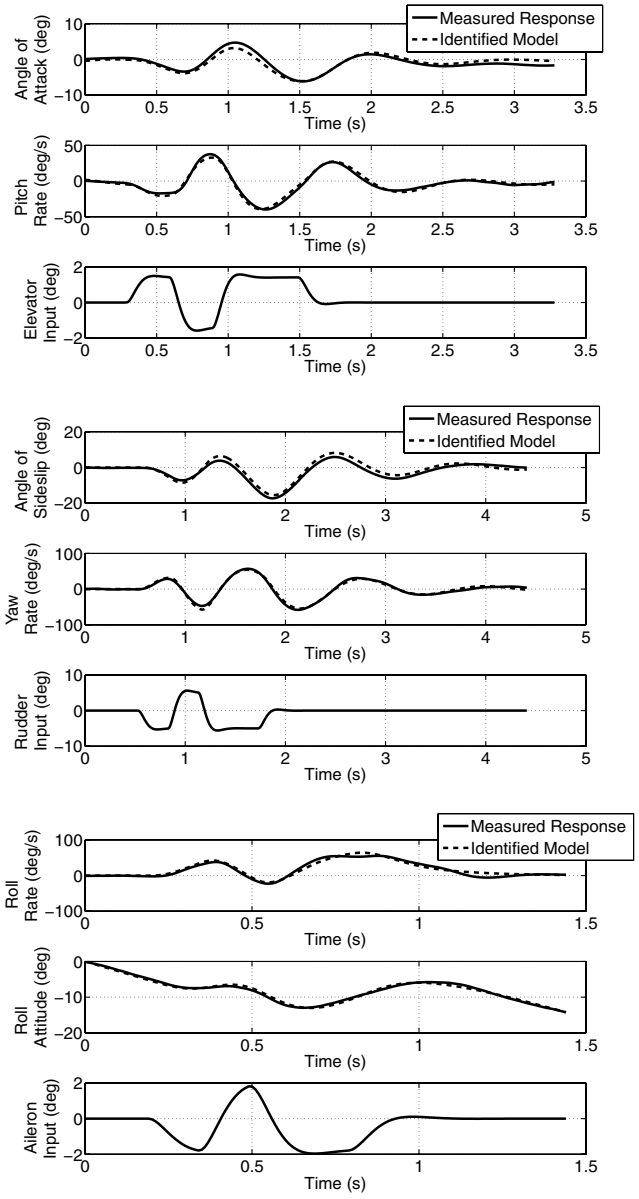

Fig. 12 Comparison of measured and predicted responses for 1-1-2 inputs to the elevator, rudder, and ailerons.

two full sinusoidal waveforms. The upper limit was selected so that the model dynamics of interest were included in the frequency band and was typically chosen as 3 Hz. A resolution of 0.02 Hz was used.

In the frequency domain, the state space equations of motion incorporating a time delay can be written as

$$j\omega_k \tilde{\mathbf{x}}(\omega_k) = \mathbf{A}\tilde{\mathbf{x}}(\omega_k) + \mathbf{B}\tilde{\mathbf{u}}(\omega_k)e^{-j\omega_k\tau} \tag{14}$$

$$\tilde{\mathbf{y}}(\omega_k) = \mathbf{C}\tilde{\mathbf{x}}(\omega_k) + \mathbf{D}\tilde{\mathbf{u}}(\omega_k)e^{-j\omega_k\tau} \tag{15}$$

$$\tilde{\mathbf{z}}(\omega_k) = \tilde{\mathbf{y}}(\omega_k) + \tilde{\mathbf{v}}(\omega_k) \qquad k = 1, 2, \ldots, N \tag{16}$$

where the tilde denotes a variable transformed into the frequency domain and ω_k is the vector of N discrete frequencies in rad/s. The vector $\mathbf{x}$ contains the aircraft states, $\mathbf{y}$ is the output vector, $\mathbf{u}$ is the input vector, and τ is a vector of time delays for each of the control inputs. The vector $\mathbf{z}$ contains measured values of the elements of $\mathbf{y}$ corrupted by the noise vector $\mathbf{v}$. The elements of $\mathbf{v}$ are assumed to be independent, Gaussian random variables with zero mean. The system matrices $\mathbf{A}$, $\mathbf{B}$, $\mathbf{C}$, and $\mathbf{D}$ contain the stability and control derivatives.

Parameter estimation was attempted using the equation error and output error methods [17]. It was not possible to solve the equation error problem using linear regression as the equivalent time delay term made the estimation problem a nonlinear one. Hence, the modified Newton–Raphson technique, normally applied in the output error formulation, was used for both methods. As this algorithm is iterative, it required specification of initial values for the unknown parameters.

A detailed mathematical description of the modified Newton–Raphson technique and its application in frequency domain estimation is not given here. The interested reader can find this material covered in Klein and Morelli [17]. A brief summary of the important relationships in the algorithm, however, is given below. The cost function to be minimized is

$$J(\Theta) = N\sum_{k=1}^{N} \tilde{\nu}^{\dagger}(\omega_k, \Theta)\mathbf{S}_{\mathbf{vv}}^{-1}\tilde{\nu}(\omega_k, \Theta) + N\,\ell_n\,|\mathbf{S}_{\mathbf{vv}}| \tag{17}$$

where ν are the residuals and $\mathbf{S}_{\mathbf{vv}}$ is a real diagonal matrix whose elements are the power spectral densities of the elements of $\mathbf{v}$. The dagger symbol denotes the complex conjugate transpose. In the formulation of the equation error method, the state derivatives are treated as the measured values, that is,

$$\tilde{\mathbf{z}}(\omega_k) = j\omega_k\tilde{\mathbf{x}}(\omega_k) \tag{18}$$

and the residuals are defined as

$$\tilde{\nu}(\omega_k) = \tilde{\mathbf{z}}(\omega_k) - \mathbf{A}\tilde{\mathbf{x}}(\omega_k) + \mathbf{B}\tilde{\mathbf{u}}(\omega_k) \tag{19}$$

For the output error method, the residuals are

$$\tilde{\nu}(\omega_k) = \tilde{\mathbf{z}}(\omega_k) - \tilde{\mathbf{y}}(\omega_k) \tag{20}$$

and an estimate of the power spectral density matrix is obtained from

$$\hat{\mathbf{S}}_{\mathbf{vv}} = \sum_{k=1}^{N} \tilde{\nu}(\omega_k, \hat{\Theta})\tilde{\nu}^{\dagger}(\omega_k, \hat{\Theta}) \tag{21}$$

The vector of parameter estimates for the ith iteration is calculated from

$$\hat{\Theta}_i = \hat{\Theta}_{i-1} + \Delta\Theta \tag{22}$$

where the parameter update is given by

$$\Delta\Theta = -\left[\frac{\partial^2 J(\Theta)}{\partial\Theta\partial\Theta^T}\right]^{-1}\left[\frac{\partial J(\Theta)}{\partial\Theta}\right] \tag{23}$$

Convergence is achieved and the process is halted when the relative change in the cost function from one iteration to the next falls below a user-defined threshold.

VII. Results of Analysis of One-Twelfth Scale BAe Hawk Model

The results presented in this section were obtained using three maneuvers: a 3-2-1-1 input to the elevator, a 3-2-1-1 input to the rudder, and a doublet input to the ailerons. First, the data compatibility check was carried out on each segment of data. An attempt was made initially to estimate a bias and a scale factor error for both the attitude and rate measurements. However, the attitude errors were found to have large variances and were highly correlated with the gyro errors. The removal of the attitude errors from the analysis also had little effect on the resulting match between the measured and reconstructed attitudes. Hence, the attitudes were treated as being error free and the data compatibility check focused on the estimation of the gyro parameters. Using the form of Eq. (12), the linearized kinematic equations of interest were

$$\dot{\phi} = (p_m - b_p)/(1 + \lambda_p) \tag{24}$$

$$\dot{\theta} = (q_m - b_q)/(1 + \lambda_q) \tag{25}$$

$$\dot{\psi} = (r_m - b_r)/(1 + \lambda_r) \tag{26}$$

Estimates of the scale factor and bias errors in Eqs. (24–26) are given in Table 1. These were obtained using the time domain output error method, which was found to perform well despite some noise being present in the gyro measurements. For comparison, the analysis was repeated but with the gyro data smoothed beforehand using a Fourier

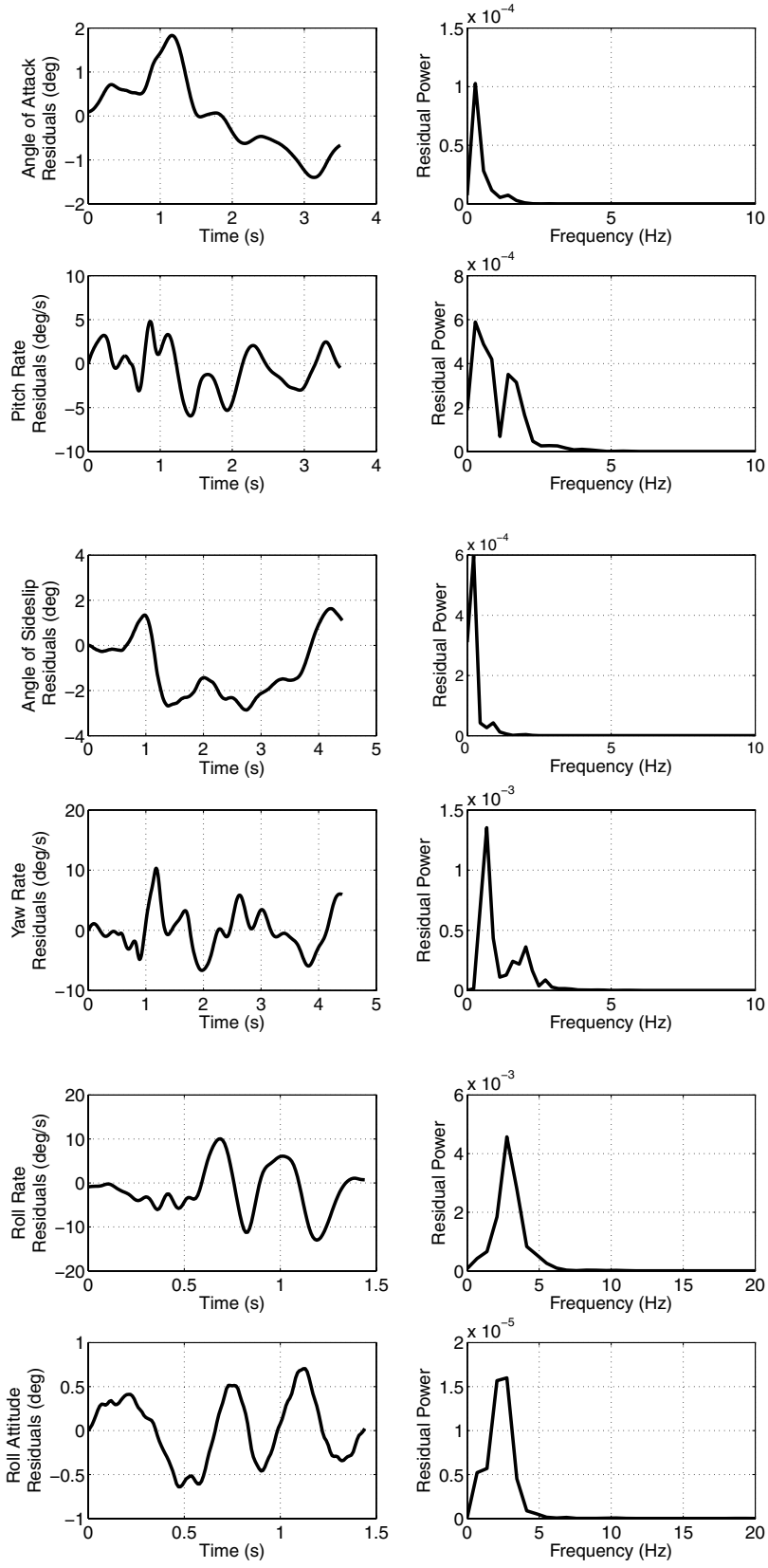

Fig. 13 Prediction residuals and associated power spectrums.

smoothing technique [25]. The results matched very closely with those obtained using the unsmoothed gyro data. Standard errors of the estimates are also given in Table 1, with the metric displayed in the last column as a percentage of the estimated parameter value. Note that the standard errors are found from the square root of the diagonal elements of the Cramer–Rao lower bound [17]. Time histories of the measured and reconstructed attitudes are shown in Figs. 7–9 and, as can be seen, a close match was obtained between the two for each of the angles.

Table 2 shows the results of the parameter estimation process. As mentioned above, starting estimates of the derivatives were required to initiate the procedure. However, the equation error method is known to be more robust to the starting values of the parameters [17] in comparison with the output error method and it was found that the initial estimates could all be set to zero without affecting convergence. The values given in Table 2 are the final parameter estimates from the output error method and, again, the standard errors of the estimates are displayed. Note that for the elevator and rudder input data, the wind-tunnel velocity term V_T, appearing in Eqs. (2) and (4), was also treated as an unknown parameter to be estimated. Pairwise correlation coefficients between the parameters for the three data segments are given in Tables 3–5.

Overall, the results are promising. The standard errors for all the parameters were reasonably low, indicating a high level of confidence in the estimates. Tables 3–5 also show that the correlation coefficients were acceptable as no coefficient value exceeded 0.9—the value at which two parameters can be considered to be highly correlated [17,19]. In Fig. 10, time histories of the measured output variables are plotted against responses generated using the identified model. For each of the variables, there was a close match between the measured and identified responses. The modeling residuals and their associated power spectrums for each of the output variables are then shown in Fig. 11. The residual power was generally concentrated in the low frequency regions below 5 Hz, corresponding to the rigid-body dynamics, and indicated that the residuals were due to small deterministic modeling errors.

For interest, theoretical estimates of the stability and control derivatives, obtained from empirical analysis [5], are also displayed in Table 1. The majority of the experimental and theoretical values matched each other to within 15%. The exceptions to this were in the estimates of the roll derivatives, l_p and l_ξ, and the directional stability derivative n_v, where the discrepancies were closer to 30%.

To validate the output error parameter estimates in Table 2, the identified model was then used to predict the response to a different input. For this purpose, three data segments, each containing a 1-1-2 input to one of the control surfaces, were used. Time histories of the measured and predicted responses for the given inputs are shown in Fig. 12. In each case, the predicted response matched closely to the measurements. Prediction residuals and their power spectrums are also depicted in Fig. 13. In comparison to the modeling residuals in Fig. 11, the prediction residuals were of roughly the same magnitude and the residual power was again concentrated in the low frequency band associated with the rigid-body dynamics. The match in magnitude and character of the modeling and prediction residuals suggests that the identified model was adequate for describing the dynamics of the one-twelfth scale Hawk.

VIII. Conclusions

This paper has presented a process of determining the stability and control characteristics of small-scale aircraft from wind-tunnel experiments which aim to emulate flight tests. The scaled aircraft are flown in semifree flight and their motion is recorded using an inertial measurement unit using MEMS sensor technology. The results from the analysis of a one-twelfth scale BAe Hawk model were also outlined. A simple multistep input approach was found to work well for exciting the model dynamics provided the input type was adjusted to prevent excessive off-axis response. Although control surface deflections could not be measured directly, due to size constraints, they were inferred successfully using knowledge of actuator dynamics and the control linkages obtained from bench tests. Before parameter estimation, a data compatibility check was performed to ensure that the angular rates and attitudes were kinematically consistent and to obtain estimates of the bias and scale factor errors in the gyro measurements. Despite the presence of some noise, the maximum likelihood output error method estimated the gyro errors adequately as shown by the close match obtained between the measured and reconstructed attitude time histories. Parameter estimation was carried out using the equation error and output error formulations in the frequency domain as there was a need to estimate time delay parameters and to remove the effects of a high-frequency structural vibration from the data. The results of the parameter estimation process were promising, with the final estimates having low standard errors and satisfactory correlation coefficients. To validate the parameter estimates, the identified model was also used to predict the response to a different input. The resulting prediction residuals were of similar magnitude and character to the modeling residuals, indicating that the identified model was adequate for describing the dynamics of the one-twelfth scale Hawk.

Acknowledgments

The authors wish to thank the Engineering and Physical Science Research Council (EPSRC) and BAE Systems for funding this research. In particular, the continued encouragement and support of Chris Fielding from BAE Systems is gratefully acknowledged.

References

[1] Orlik-Ruckemann, K., "Review of Techniques for Determination of Dynamic Stability Parameters in Wind Tunnels," AGARD LS-114, 1981, Paper 3.

[2] Bennett, R. M., Farmer, M. G., Mohr, R. L., and Hall, E. W., "Wind Tunnel Technique for Determination of Dynamic Stability Derivatives from Cable-Mounted Models," *Journal of Aircraft*, Vol. 15, No. 5, 1978, pp. 304–309. doi:10.2514/3.5836010.2514/3.58360

[3] Subke, H., "Test Installations to Investigate the Dynamic Behaviour of Aircraft with Scaled Models in Wind Tunnels," *Transactions of the Institute of Measurement and Control (London)*, Vol. 1, No. 3, 1979, pp. 135–140. doi:10.1177/014233127900100302

[4] Krag, B., "The Wind Tunnel Behaviour of a Scaled Model with a Gust Alleviation System in a Deterministic Gust Field," *Transactions of the Institute of Measurement and Control (London)*, Vol. 1, No. 3, 1979, pp. 141–153. doi:10.1177/014233127900100303

[5] Malik, I. A., "The Design, Development and Evaluation of an Active Control Aircraft Model Wind Tunnel Facility," Ph.D. Thesis, College of Aeronautics, Cranfield Institute of Technology, Cranfield, England, U.K., 1982.

[6] Heydari, F., "On the Estimation of Stability and Control Characteristics of a Generalised Forward Swept Wing Aircraft," Ph.D. Thesis, College of Aeronautics, Cranfield Institute of Technology, Cranfield, England, U.K., 1986.

[7] Cook, M. V., "On the Use of Small Scale Aircraft Models for Dynamic Wind Tunnel Investigation of Stability And Control," *Transactions of the Institute of Measurement and Control (London)*, Vol. 9, No. 4, 1987, pp. 190–197. doi:10.1177/014233128700900405

[8] Hinds, H. A., "The Application of a Modified Stepwise Regression (MSR) Method to the Estimation of Aircraft Stability and Control Derivative," Ph.D. Thesis, College of Aeronautics, Cranfield Institute of Technology, Cranfield, England, U.K., 1996.

[9] Rajamurthy, M. S., "Generation of Comprehensive Longitudinal Aerodynamic Data Using Dynamic Wind-Tunnel Simulation," *Journal of Aircraft*, Vol. 34, No. 1, 1997, pp. 29–33. doi:10.2514/2.2157

[10] Yadzi, N., Ayazi, F., and Najafi, K., "Micromachined Inertial Sensors," *Proceedings of the IEEE*, Vol. 86, No. 8, 1998, pp. 1640–1659. doi:10.1109/5.704269

[11] "USAF Stability and Control DATCOM," Flight Control Division, U.S. Air Force Flight Dynamics Laboratory, Wright–Patterson Air Force Base, Fairborn, OH.

[12] ESDU, "Aerodynamics Series," Engineering Sciences Data Unit, ESDU International, London.

[13] Kumar, H., "A Preliminary Study into the Design of a Free Flight Wind Tunnel Model for Demonstrating the Dynamic Characteristics of Aircraft," M.S. Thesis, College of Aeronautics, Cranfield Institute of Technology, Cranfield, England, U.K., 1980.

[14] Gebre-Egziabher, D., Hayward, R. C., and Powell, J. D., "Design of Multi-Sensor Attitude Determination Systems," *IEEE Transactions on Aerospace and Electronic Systems*, Vol. 40, No. 2, 2004, pp. 627–649. doi:10.1109/TAES.2004.1310010

[15] Cook, M. V., *Flight Dynamics Principles*, Edward Arnold, London, 1997.

[16] Filmer, S. W., "Artificial G Control System for the Dynamic Wind Tunnel Facility," M.Sc. Thesis, College of Aeronautics, Cranfield Institute of Technology, Cranfield, England, U.K., 1989.

[17] Klein, V., and Morelli, E. A., *Aircraft System Identification: Theory and Practice*, AIAA, Reston, VA, 2006.

[18] Morelli, E. A., "System Identification Programs for Aircraft (SIDPAC)," AIAA Paper 2002-4704, Aug. 2002.

[19] Jategaonkar, R. V., *Flight Vehicle System Identification: A Time Domain Methodology*, AIAA, Reston, VA, 2006.

[20] Theodore, C. R., Tischler, M. B., and Colbourne, J. D., "Rapid Frequency Domain Modeling Methods for UAV Flight Control Applications," *Journal of Aircraft*, Vol. 41, No. 4, 2004, pp. 735–743. doi:10.2514/1.4671.doi:.

[21] Mulder, J. A., Sridhar, J. K., and Breeman, J. H., "Identification of Dynamic Systems—Application to Aircraft," AGARD AG-300, Vol. 3, Pt. 2, 1994.

[22] Steers, S. T., and Iliff, K. W., "Effects of Time-Shifted Data on Flight-Determined Stability and Control Derivatives," NASA TN-D-7830, March 1975.

[23] Tischler, M. B., and Remple, R. K., *Aircraft and Rotorcraft System Identification: Engineering Methods with Flight Test Examples*, AIAA, Reston, VA, 2006.

[24] Marchand, M., and Fu, K. H., "Frequency Domain Parameter Estimation of Aeonautical Systems Without and With Time Delays," *Proceedings of the 7th IFAC Symposium on Identification and System Parameter Estimation*, Pergamon, Oxford, U.K., July 1985, pp. 669–674.

[25] Morelli, E. A., "Estimating Noise Characteristics from Flight Test Data Using Optimal Fourier Smoothing," *Journal of Aircraft*, Vol. 32, No. 4, 1995, pp. 689–695. doi:10.2514/3.4677810.2514/3.46778